Pergamon

Int. J. Heat Mass Transfer. Vol. 38, No. 14, pp. 2529–2537, 1995

0017-9310/95 $9.50 + 0.00

0017-9310(95)00020-8

Heat transfer by oscillating flow in a circular pipe with a sinusoidal wall temperature distribution

DAE-YOUNG LEE, SANG-JIN PARK and SUNG TACK RO†

Department of Mechanical Engineering, Seoul National University, Seoul 151-742, Korea

(*Received* 20 *April* 1994 *and in final form* 19 *December* 1994)

Abstract—A theoretical investigation was carried out on the heat transfer characteristics of an oscillating flow in a circular pipe. In contrast with the earlier studies on similar topics, the nonlinear temperature boundary condition, more precisely sinusoidal temperature distribution, was considered in this study. For this specific case, the present study revealed the existence of two important parameters and the occurrence of three distinct regimes. The detailed characteristics of the section-averaged temperature, the wall heat flux and the Nusselt number are presented and addressed. Since the general distribution of the temperature at the cylinder wall can be expanded in a Fourier series, it is of fundamental nature to analyze the case with sinusoidal temperature distribution. The superposition principle would then allow for the use of present basic analysis for more practical systems.

1. INTRODUCTION

The mass transfer augmentation in the axial direction due to pulsatile or oscillatory flow in a duct has been discussed by Chatwin [1] and Watson [2] among many others. These studies have provided much useful information in understanding transport phenomena in the respiratory and circulatory organs of the human body. Based on the analogy between heat and mass transfer, Kurzweg [3–5] observed that oscillatory flows in the tube or channel also enhance the longitudinal heat transfer for the case of a constant wall temperature gradient. In his work, the augmentation of axial heat transfer is caused not only by the two dimensionality of the velocity profile which enhances the mass transfer, but also by the periodic heat absorption–release effect of the duct wall. Later, Gedeon [6] derived the friction coefficients and the heat transfer coefficients using the solution of Kurzweg [4] and showed that there occurs a phase lag between temperature difference and heat flux at a high frequency oscillation within a parallel-plate channel. Lee [7] had formerly investigated a phenomenon similar to the result of Gedeon through the analysis on the unsteady heat transfer in a cylinder with periodically varying pressure.

Peattie and Budwig [8] measured the effective axial heat conductivity in a pipe the radius of which varies along the axis. Considering the viscous dissipation and the finite wall thickness, Kaviany [9] observed the longitudinal heat diffusion by oscillatory flow in a pipe.

A recent interest in the Stirling-cycle machines brings the results of these studies into a main stream of analyses on the Stirling-cycle machines. Kornhauser and Smith [10] applied the results of Gedeon [6], Lee [7] and so forth to the analysis on the gas spring of a free-piston Stirling engine. The studies of Lee [7] and Kornhauser and Smith [10] are further extended by Wang and Smith [11] to account for the heat transfer losses at cylinders. The above-mentioned studies however considered the cases of nearly isothermal or adiabatic outer surfaces. In these cases, the solid walls have linear temperature profiles. Practically, the wall of the heat exchanger in a Stirling-cycle machine is not adiabatic or isothermal but exposed to a nonlinear temperature condition. Furthermore, the heat transfer in these heat exchangers is governed not only by the oscillation frequency but also by the swept length of the fluid. Nevertheless most of the above-mentioned studies focus mainly on the effect of the oscillation frequency. As a result, the earlier studies on the Stirling-cycle machines are of limited applicability because neither the nonlinear temperature distribution nor the influence of the swept length was accounted for.

For the practicality, an investigation of the heat transfer at the heat exchangers of a Stirling-cycle machine should take account into the case where the axial gradient of the wall temperature varies along the longitudinal direction. In addition, both the mean temperature difference and the Nusselt number should be obtained as a function of the swept length as well as the oscillation frequency.

In the present work, the heat transfer characteristics of an oscillating pipe flow with sinusoidal wall temperature distributions are analyzed, and the influences of the oscillation frequency and the ratio of the swept

†Author to whom correspondence should be addressed.

NOMENCLATURE

$C_{n,k}$ function of λ defined in equation (18)
Cr thermal capacity ratio of fluid to wall defined in equation (A12)
c_p specific heat [J/kg°C]
g_k temperature profile function defined in equation (19)
g_f temperature profile function of fluid defined in equation (A2)
g_w temperature profile function of wall defined in equation (A3)
h_n temperature profile function defined in equation (14)
i imaginary number, $\sqrt{-1}$
L_c conduction length scale, $\omega L_s R^2/\kappa$ [m]
L_s swept length [m]
L_w period of sinusoidal wall temperature distribution [m]
Nu_D Nusselt number
Pr Prandtl number
q_a dimensionless advected energy
q_w dimensionless wall heat flux defined in equation (24)
R inner radius of pipe [m]
R_o outer radius of pipe [m]
r radial coordinate [m]
T temperature [°C]
T_a amplitude of sinusoidal wall temperature distribution [°C]
u velocity [m s^{-1}]
x dimensionless axial coordinate, $2\pi z/L_w$
z axial coordinate [m].

Greek symbols
α Womersley number, $R\sqrt{\omega/\nu}$
β modified Womersley number, $\alpha\sqrt{Pr}$
δ ratio of wall thickness to inner radius of pipe
γ axial gradient of wall temperature distribution [°C m^{-1}]
η dimensionless radial coordinate, r/R
κ thermal diffusivity [m^2 s^{-1}]
λ swept length ratio, $\pi L_s/2L_w$
μ thermal conductivity ratio of fluid to wall
ν kinematic viscosity [m^2 s^{-1}]
θ dimensionless temperature, T/T_a
ρ density [kg m^{-3}]
σ thermal diffusivity ratio of fluid to wall
τ dimensionless time, ωt
ξ dimensionless axial coordinate fixed to a fluid element, $x-2\lambda\sin\tau$.

Superscripts
Real[ ] real component of a complex number
$\langle\ \rangle$ section averaged quantity, $\langle f\rangle = \int_A f\,dA/A$
$\bar{}$ time averaged quantity, $\bar{f} = \int_0^{2\pi} f\,d\tau/2\pi$
$'$ radial gradient at $\eta = 1, f' = df/d\eta(1)$
$*$ complex conjugate.
o renormalized quantities.

Subscripts
f fluid
w wall.

length to the characteristic length of the wall boundary condition have been investigated. In our theoretical approach the two dimensional (2D) unsteady energy equation is solved with an assumption of a uniform axial velocity at a cross section. The uniform velocity profile corresponds to a limiting case of $Pr \ll 1$ and the heat transfer characteristics in this case do not deviate much from those for a moderate value of Pr, as evidenced in Fig. 1. Figure 1 depicts the advected energy in a cycle by an oscillating flow subjected to a linear wall temperature distribution, which is originally obtained by Kurzweg [5] and reconstructed here in terms of β ($\beta = \alpha\sqrt{Pr}$, where $\alpha = R\sqrt{\omega/\nu}$ is the Womersley number). From this figure, it is noted that for a fixed value of β the dependence of the advected energy on Prandtl number is not great for $Pr < 1$. Consequently, the solution with uniform velocity assumption can successfully predict the heat transfer in real situations with 2D velocity profile. The validity of this assumption is discussed more precisely in the Appendix.

The outcome of the present analysis is expected to provide basic information on the effect of the swept length and explain the characteristics of the heat transfer with nonlinear wall temperature distributions. Furthermore, this investigation with sinusoidal temperature distribution can figure out several key features of the practical heat transfer with the temperature conditions of general types when aided by the superposition principle, because the general tem-

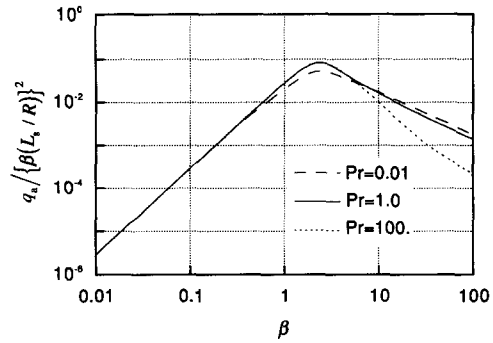

Fig. 1. Advected energy with respect to the modified Womersley number in the case of $Cr \to \infty$.

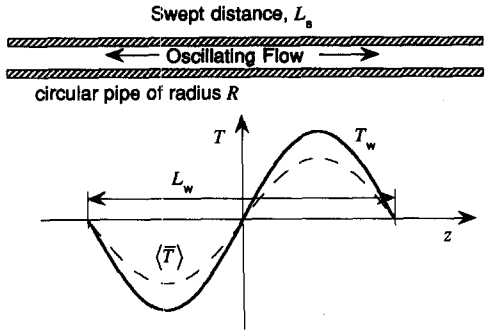

Fig. 2. Oscillating flow in a circular pipe subjected to a sinusoidal wall temperature distribution.

perature distribution can be expanded in a Fourier series.

2. ANALYSIS

Consider an infinitely long circular cylinder of radius R, the wall temperature of which is uniform circumferentially but varies in a sinusoidal manner along the axis, as shown in Fig. 2. A fluid entrapped in the cylinder oscillates with a given frequency by means of a certain external force. The oscillating flow and relevant heat transfer are considered to be laminar and repeating periodically. Strictly speaking, the wall temperature is prone to fluctuate from its imposed profile in response to the flow oscillation. However, Kaviany [9] suggests that when the heat capacity of the wall is much larger than that of the fluid the timewise variation of the wall temperature at a given cross section is negligibly small. Therefore, it is reasonable to assume that the wall temperature is independent of time and remains at its sinusoidal distribution. The validity of this assumption is more rigorously assessed in this study and the detailed discussion is presented in the Appendix.

The present work aims at analyzing the influence of longitudinally nonlinear distribution of wall temperature on the heat transfer. As mentioned earlier, the results so obtained will serve as a fundamental tool to deal with general nonlinear temperature conditions with the aid of the superposition principle.

Particularly, we restrict our attention to the case of $L_w \gg R$ (see Fig. 2). Then, the governing equation may be simplified as

$$\frac{\partial T}{\partial t}+u\frac{\partial T}{\partial z}=\kappa\frac{1}{r}\frac{\partial}{\partial r}\left(r\frac{\partial T}{\partial r}\right)$$

$$\left.\frac{\partial T}{\partial r}\right|_{r=0}=0 \quad T|_{r=R}=T_a\sin(2\pi z/L_w) \tag{1}$$

where L_w is the characteristic length of the wall temperature distribution. In the above, the axial conduction was neglected considering $L_w \gg R$.

Now, we assume that the radial distribution of the velocity is uniform as discussed previously. For the present problem, the swept length of the fluid, L_s, plays an important role of process parameter. Hence, for a given L_s, a constraint, $\int_0^{2\pi/\omega}|u|\,dt = 2L_s$, can be utilized in constructing the transient velocity field, which yields

$$u=\frac{L_s\omega}{2}\cos\omega t \tag{2}$$

where ω represents the angular frequency of the flow oscillation.

Next, the governing equation and boundary conditions are rendered dimensionless by introducing the following quantities:

$$\theta=\frac{T}{T_a} \quad \tau=\omega t \quad x=2\pi\frac{z}{L_w} \quad \eta=\frac{r}{R}. \tag{3}$$

Equation (1) then becomes

$$\beta^2\frac{\partial\theta}{\partial\tau}+2\beta^2\lambda\cos\tau\frac{\partial\theta}{\partial x}=\frac{1}{\eta}\frac{\partial}{\partial\eta}\left(\eta\frac{\partial\theta}{\partial\eta}\right) \tag{4}$$

$$\left.\frac{\partial\theta}{\partial\eta}\right|_{\eta=0}=0 \quad \theta|_{\eta=1}\equiv\theta_w=\sin x \tag{5}$$

where

$$\beta=R\sqrt{\frac{\omega}{\kappa}} \quad \lambda=\frac{\pi L_s}{2L_w}. \tag{6}$$

Obviously, two important dimensionless numbers, i.e. β and λ, are introduced; β stands for the modified Womersley number ($\beta=\alpha\sqrt{Pr}$, where α is the Womersley number) which is a ratio of the radius to the thickness of the Stokes' thermal boundary layer, and λ is associated with a ratio of the swept length to the characteristic length of wall temperature distribution. Conceptually, β and λ represent two different aspects of the flow oscillation, i.e. how frequent or how far is the flow oscillation.

Equations (4) and (5) can be converted into more tractable forms by employing a Lagrangian coordinate

$$\xi\equiv x-2\lambda\sin\tau. \tag{7}$$

As a result of transformation, we have

$$\beta^2\frac{\partial\theta}{\partial\tau}=\frac{1}{\eta}\frac{\partial}{\partial\eta}\left(\eta\frac{\partial\theta}{\partial\eta}\right) \tag{8}$$

$$\left.\frac{\partial\theta}{\partial\eta}\right|_{\eta=0}=0 \quad \theta|_{\eta=1}=\theta_w=\sin(\xi+2\lambda\sin\tau). \tag{9}$$

The exact solution to equations (8) and (9) can be determined from the Fourier analysis, or

$$\theta=\mathrm{Real}\left[\sum_{n=0}^{\infty}\theta_n\,e^{in\tau}\right]. \tag{10}$$

The boundary condition (9) is also expanded in a Fourier series, using the special formulae listed below [12],

$$[\cos(2\lambda\sin\tau) = J_0(2\lambda) + 2\sum_{k=1}^{\infty} J_{2k}(2\lambda)\cos(2k\tau)]$$

$$\sin(2\lambda\sin\tau) = 2\sum_{k=1}^{\infty} J_{2k-1}(2\lambda)\sin\{(2k-1)\tau\} \quad (11)$$

such that

$$\theta_w = (\sin\xi)J_0(2\lambda) + 2\,\mathrm{Real}\left[\sin\xi\sum_{n=1}^{\infty} J_{2n}(2\lambda)\,e^{i2n\tau} - i\cos\xi\sum_{n=1}^{\infty} J_{2n-1}(2\lambda)\,e^{i(2n-1)\tau}\right] \quad (12)$$

where $J_n(x)$ is the first kind of Bessel function of order n.

Substituting equation (10) into equation (8) and imposing the boundary condition equation (11), we have

$$\theta = (\sin\xi)J_0(2\lambda) + 2\,\mathrm{Real}\left[\sin\xi\sum_{n=1}^{\infty} h_{2n}J_{2n}(2\lambda)\,e^{i2n\tau} - i\cos\xi\sum_{n=1}^{\infty} h_{2n-1}J_{2n-1}(2\lambda)\,e^{i(2n-1)\tau}\right] \quad (13)$$

where

$$h_n \equiv \frac{I_0(\beta\sqrt{in\eta})}{I_0(\beta\sqrt{in})} \quad (14)$$

and $I_n(z)$ is the first kind of the modified Bessel function of order n. Though expressed in a compact form, the above solution needs to be rephrased with respect to x and τ for the purpose of time- and section-averaging at a given fixed point. Therefore, equation (13) is transformed into the Eulerian form merely by letting $\xi = x - 2\lambda\sin\tau$ in equation (13), to yield

$$\theta = \sin(x-2\lambda\sin\tau)J_0(2\lambda) + 2\,\mathrm{Real}\left[\sin(x-2\lambda\sin\tau)\sum_{n=1}^{\infty} h_{2n}J_{2n}(2\lambda)\,e^{i2n\tau} - i\cos(x-2\lambda\sin\tau)\sum_{n=1}^{\infty} h_{2n-1}J_{2n-1}(2\lambda)\,e^{i(2n-1)\tau}\right]. \quad (15)$$

In order to sort out the terms corresponding to each frequency n, equation (15) is expanded again in a Fourier series with respect to τ. This gives

$$\theta = (\sin x)J_0^2(2\lambda) + 2\,\mathrm{Real}\left[\sin x\sum_{m=1}^{\infty} J_m^2(2\lambda)h_m\right] + \mathrm{Real}\sum_{n=1}^{\infty}\left[\sin x\left\{2J_0J_{2n} + 2\sum_{m=1}^{\infty} J_m(J_{m-2n}h_m + J_{m+2n}h_m^*)\right\}e^{i2n\tau} + i\cos x\left\{2J_0J_{2n-1} + 2\sum_{m=1}^{\infty} J_m(J_{m+(2n-1)}h_m^* - J_{m-(2n-1)}h_m)\right\}e^{i(2n-1)\tau}\right] \quad (16)$$

where the asterisks denote complex conjugates. After some manipulations, equation (16) becomes

$$\theta = \sin x + \mathrm{Real}\left[\sum_{k=1}^{\infty} C_{0,k}\,g_k\sin x + \sum_{n=1}^{\infty}\left\{\sum_{k=-\infty,k\neq 0}^{\infty} C_{2n,k}g_k\,e^{2ni\tau}\sin x + i\sum_{k=-\infty,k\neq 0}^{\infty} C_{2n-1,k}g_k\,e^{(2n-1)i\tau}\cos x\right\}\right] \quad (17)$$

with

$$C_{n,k} \equiv (-1)^{k+1}2J_k(2\lambda)J_{n-k}(2\lambda) \quad (18)$$

$$g_k \equiv 1 - \frac{I_0(\beta\sqrt{ik\eta})}{I_0(\beta\sqrt{ik})}. \quad (19)$$

The final solution so obtained can be differentiated with respect to the radial coordinate or integrated over the section and/or time to identify the heat transfer characteristics. Based on these solutions, we will introduce a few different regimes according to the parameter values.

3. RESULTS AND DISCUSSION

3.1. *Definitions*

For convenience of presentation, a few useful quantities are derived from the foregoing solutions.

(1) *Section-averaged fluid temperature*, $\langle\theta\rangle$, is simply obtained by integrating equation (17) over the cross-section:

$$\langle\theta\rangle = \sin x + \mathrm{Real}\left[\sum_{k=1}^{\infty} C_{0,k}\langle g_k\rangle\sin x + \sum_{n=1}^{\infty}\left\{\sum_{k=-\infty,k\neq 0}^{\infty} C_{2n,k}\langle g_k\rangle\,e^{2ni\tau}\sin x + i\sum_{k=-\infty,k\neq 0}^{\infty} C_{2n-1,k}\langle g_k\rangle\,e^{(2n-1)i\tau}\cos x\right\}\right] \quad (20)$$

where $\langle g_k\rangle$ designates the section-average of g_k

$$\langle g_k\rangle = 1 - \frac{2}{\beta\sqrt{ik}}\frac{I_1(\beta\sqrt{ik})}{I_0(\beta\sqrt{ik})}. \quad (21)$$

This function has two asymptotes:

$$\langle g_k\rangle \approx \begin{cases} \frac{1}{48}k^2\beta^4 + i\frac{1}{8}k\beta^2 & \text{as } \beta\to 0 \\ 1 & \text{as } \beta\to\infty \end{cases}. \quad (22)$$

(2) *Section-time-averaged fluid temperature*, $\langle\bar{\theta}\rangle$, is also obtained by further integrating equation (20) over the oscillation period (or simply by dropping out the unsteady terms of $e^{in\tau}$):

$$\langle\bar{\theta}\rangle = \sin x + \mathrm{Real}\left[\sum_{k=1}^{\infty} C_{0,k}\langle g_k\rangle\sin x\right]. \quad (23)$$

(3) *Wall heat flux*, q_w, is derived by differentiating

equation (17) with respect to η and evaluating it at $\eta = 1$:

$$q_w = \left.\frac{\partial\theta}{\partial\eta}\right|_{\eta=1}$$

$$= \mathrm{Real}\left[\sum_{k=1}^{\infty} C_{0,k} g_k' \sin x + \sum_{n=1}^{\infty}\left\{\sum_{k=-\infty,k\neq 0}^{\infty} C_{2n,k} g_k' \, e^{2ni\tau} \sin x + i \sum_{k=-\infty,k\neq 0}^{\infty} C_{2n-1,k} g_k' \, e^{(2n-1)i\tau} \cos x\right\}\right] \quad (24)$$

where $g_k' \equiv dg_k/d\eta(1)$. From equation (19), g_k' becomes

$$g_k' = -\beta\sqrt{ik}\frac{I_1(\beta\sqrt{ik})}{I_0(\beta\sqrt{ik})}. \quad (25)$$

Similar to equation (22), it can be shown that g_k' is asymptotically expressed as

$$g_k' \approx \begin{cases} -\frac{1}{16}k^2\beta^4 - i\frac{1}{2}k\beta^2 & \text{as } \beta \to 0 \\ -\beta\sqrt{k/2} - i\beta\sqrt{k/2} & \text{as } \beta \to \infty \end{cases}. \quad (26)$$

(4) *Time-averaged heat flux*, $\bar{q}_w$, is derived by integrating equation (24) over the oscillation period:

$$\bar{q}_w = \mathrm{Real}\left[\sum_{k=1}^{\infty} C_{0,k} g_k' \sin x\right]. \quad (27)$$

(5) *Nusselt number*, Nu_D, is defined as

$$Nu_D = \frac{2\bar{q}_w}{\theta_w - \langle\bar{\theta}\rangle} = -2 \cdot \mathrm{Real}\left[\sum_{k=1}^{\infty} C_{0,k} g_k'\right] \Big/ \mathrm{Real}\left[\sum_{k=1}^{\infty} C_{0,k}\langle g_k\rangle\right]. \quad (28)$$

In what follows, the influence of β and λ on the above-defined quantities is addressed and physically distinct regimes are identified.

3.2. *Mean temperature*

The representative temperature difference is expressed as

$$\langle\overline{\Delta\theta}\rangle = \theta_w - \langle\bar{\theta}\rangle. \quad (29)$$

Figure 3 presents a bird's-eye view of the normalized temperature difference plotted in the β–λ plane. As can be seen in Fig. 3, $\langle\overline{\Delta\theta}\rangle$ is very small in the vicinity of $\beta = 0.1$. In fact, for small β, equation (20) is approximately reduced to

$$\langle\theta\rangle \approx \left\{1 - \tfrac{1}{24}\beta^4 \sum_{k=1}^{\infty} k^2 J_k^2(2\lambda)\right\}\sin x + \mathrm{Real}\left[i\sum_{k=-\infty}^{\infty} J_{k-1}(2\lambda)J_k(2\lambda)(\tfrac{1}{24}k^2\beta^4 + i\tfrac{1}{4}k\beta^2)\, e^{i\tau}\cos x\right] + \text{higher-frequency terms}$$

$$= (1 - \tfrac{1}{24}\beta^4\lambda^2)\sin x + \mathrm{Real}[(-\tfrac{1}{4}\beta^2\lambda + i\tfrac{1}{24}\beta^4\lambda)\, e^{i\tau}\cos x] + \text{higher-frequency terms} \quad (30)$$

or

$$\langle\overline{\Delta\theta}\rangle \approx \tfrac{1}{24}\beta^4\lambda^2 \sin x. \quad (31)$$

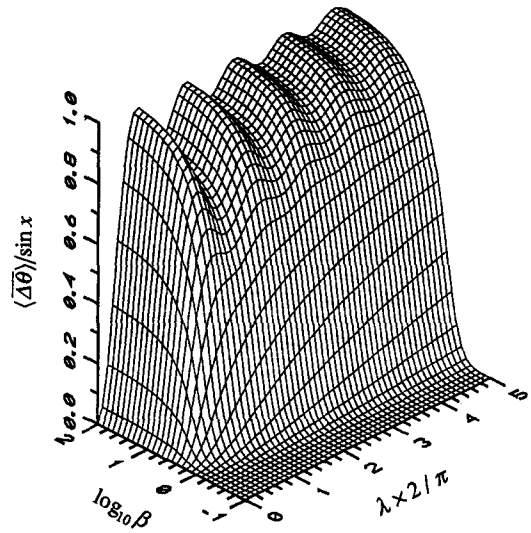

Fig. 3. Representative temperature difference.

Obviously when either β or λ is zero (i.e. fluid is at rest), equation (31) reduces to $\langle\overline{\Delta\theta}\rangle = 0$; in other words, the whole fluid is at the same temperature as the wall. Focusing only on the primary frequency response, i.e. for $n = 1$, the second term in equation (30) reveals that the amplitude of fluid temperature variation is proportional to $\beta^2\lambda\cos x$ for small β. This is qualitatively in good accord with the findings of Gedeon [6] in which the amplitude of fluid temperature variation is shown to be proportional to the product of β^2 and wall temperature gradient.

But when β is fixed to a large value, Fig. 3 indicates that the $\langle\overline{\Delta\theta}\rangle$ curve shows ridges and grooves periodically. Furthermore, for a very large β, $\langle\overline{\Delta\theta}\rangle$ undergoes oscillation with λ and converges to a well-behaved curve of $1 - J_0^2(2\lambda)$. This can be explained with the aid of equation (20). Since $\langle g_k\rangle \approx 1$ for $\beta \to \infty$, we have

$$\langle\theta\rangle \approx \sin x + \mathrm{Real}\left[\sum_{k=1}^{\infty} C_{0,k}\sin x + \sum_{n=1}^{\infty}\left\{\sum_{k=-\infty,k\neq 0}^{\infty} C_{2n,k}\, e^{2ni\tau}\sin x + i\sum_{k=-\infty,k\neq 0}^{\infty} C_{2n-1,k}\, e^{(2n-1)i\tau}\cos x\right\}\right]$$

$$= J_0^2(2\lambda)\sin x + 2J_0(2\lambda)\mathrm{Real}\left[\sum_{n=1}^{\infty}\{J_{2n}(2\lambda)\, e^{2ni\tau}\sin x\right.$$

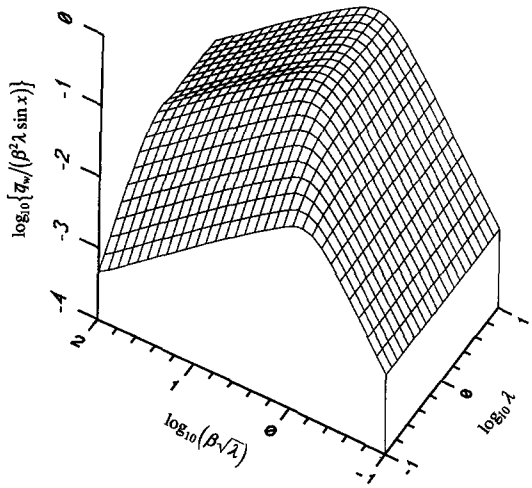

Fig. 4. Time-averaged heat flux.

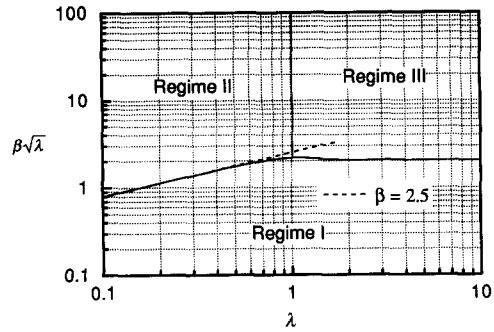

Fig. 5. Projective plot of Fig. 4.

$$+\mathrm{i}J_{2n-1}(2\lambda)\,\mathrm{e}^{(2n-1)\mathrm{i}\tau}\cos x\}\Big] \tag{32}$$

and, subsequently, we obtain by time-averaging

$$\langle\bar{\theta}\rangle \approx J_0^2(2\lambda)\sin x \tag{33}$$

from which the representative temperature difference is derived as

$$\langle\overline{\Delta\theta}\rangle \approx \{1-J_0^2(2\lambda)\}\sin x. \tag{34}$$

Equation (34) implies that, when β is sufficiently large, $\langle\overline{\Delta\theta}\rangle$ is a function of λ only. It is further interesting to interpret equation (32) from the Lagrangian point of view. This can be done just by rewriting equation (32) in a compact form

$$\langle\theta\rangle_{\text{Lagrangian}} \approx \frac{1}{2\pi}\int_0^{2\pi}\sin(\xi+2\lambda\sin\tilde{\tau})\,\mathrm{d}\tilde{\tau} \tag{35}$$

the right-hand side of which does not depend on time any more and can be interpreted as the time-average of the wall temperature experienced by a given fluid element (see equation (9)). As an element moves back and forth, it feels as if the wall temperature is varying with time. Here, the wall temperature variation perceived by an element is not a simple sinusoidal function of time any more. Equation (35) then gives the time-averaged value during one period, thereby indicating independence of the temperature of a moving element on time. Equation (35) can also be obtained directly from equation (13), which represents the fluid temperature in Lagrangian viewpoint.

From the above discussion, it can be inferred that for large β the heat transfer from the wall does not penetrate into the core part but prevails only within a thin annular space. Also, from the Lagrangian standpoint the section-averaged fluid temperature is hardly influenced by the wall conditions.

3.3. *Regime Map*

The time-averaged heat flux is calculated numerically from equation (27) and the results are shown in Fig. 4. In doing this, each coordinate scale was deliberately chosen to clarify the influence of β and λ on $\bar{q}_w$. Prior to our discussion, it may be worthy of note that a combination of β and λ was used as one of the coordinates. Actually, Fig. 4 was selected out of many trial plots owing to its lucidity. Based on this elegant plot, it was successful in identifying the presence of three distinct regimes, each of which appears as a tangential plane. The occurrence of the three regimes is also evidenced in Fig. 5, which is basically a top view of Fig. 4. For convenience, these regimes are referred to Regimes I, II and III, as shown in Fig. 5. As for the dependence of the Nusselt number on the process parameters, Fig. 6 shows a 3D plot for *Nu*. It should be recognized that two different coordinates were used depending on whether λ is less than or greater than unity. It is perceptible that the Nusselt number has a weak dependence on λ when the mixed coordinates are employed. This also substantiates the occurrence of the three distinct regimes.

As can be expected from Figs. 4 and 6, the heat transfers pertinent to each regime are substantially different from one another. Accordingly, presentation

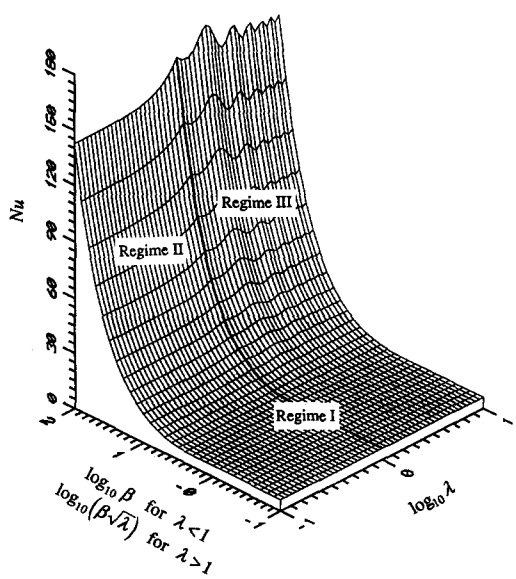

Fig. 6. Nusselt number.

of our results will be made henceforth in conjunction with the regime map.

3.4. *Heat flux and Nusselt number*

For Regime I, the asymptotic behavior of the time-averaged heat flux can be shown from equations (26) and (27). Then Nu_D can be readily obtained from this heat flux and equations (28) and (31). The results are as follows.

Regime I:

$$\bar{q}_w \approx \tfrac{1}{8}\beta^4 \sum_{k=1}^{\infty} k^2 J_k^2(2\lambda)\sin x = \tfrac{1}{8}\beta^4\lambda^2 \sin x.$$

$$Nu_D \approx 6. \tag{36}$$

For Regime II, using equations (26), (27) and (34), we can derive

Regime II:

$$\bar{q}_w \approx \sqrt{2}\beta \sum_{k=1}^{\infty} \sqrt{k} J_k^2(2\lambda)\sin x$$

$$\approx \sqrt{2}\beta\lambda^2 \sin x$$

$$Nu_D \approx 2\frac{\sqrt{2}\beta\lambda^2 \sin x}{\{1-J_0^2(2\lambda)\}\sin x} \approx \sqrt{2}\beta. \tag{37}$$

In the above, the asymptotic relations, $J_0^2(x) \approx 1-x^2/2$ and $J_1^2(x) \approx x^2/4$ for $x \ll 1$, were also used in the derivation.

For Regime III, it is not easy to deduce some kind of asymptotic formulae for $\bar{q}_w$. However, from our numerical calculation, $\bar{q}_w$ was found to be roughly proportional to $\sqrt{\lambda}$, i.e.

Regime III:

$$\bar{q}_w \approx \sqrt{2}\beta \sum_{k=1}^{\infty} \sqrt{k} J_k^2(2\lambda)\sin x$$

$$\approx 0.76\beta\sqrt{\lambda}\sin x$$

$$Nu_D \approx 1.52\beta\sqrt{\lambda}. \tag{38}$$

From these results, it is evident that $\bar{q}_w$ and thus Nu_D have different powers of dependency on β and λ in each regime. This is consistent with the presence of the regime map and may be one of the benefits of this work.

Consider a limiting case of $\lambda \ll 1$, which can be interpreted as a fluid element traveling only a short interval out of the imposed wall temperature distribution. Then, an observer moving with the element would regard the wall condition as that with a constant axial temperature gradient. For this reason, the effective axial thermal flux for the case of $\lambda \ll 1$ (obtained by integration of $\bar{q}_w$ with respect to x) was found to agree well with the results of Kurzweg [5] for $Pr \ll 1$.

3.5. *Validity of regime map*

In this section, we address the physical aspects of the regime map by taking into account the length scales of interest. First of all, it is necessary to remark here three axial length scales as below:

L_s: swept length of the oscillating flow
L_w: characteristic length associated with the sinusoidal wall temperature distribution
L_c: conduction length scale, where $L_c = (L_s\omega)(R^2/\kappa)$.

Of these three scales, L_c corresponds to the moving distance of a certain fluid element over the duration of transverse penetration time scale, (R^2/κ). This length scale is similar to the entrance length in steady unidirectional laminar flow.

For the problem considered here, it can be asserted that the shortest length scale would govern the heat transfer process. Actually, the regime map shown in Fig. 5 can be alternatively established from the scale analysis:

(i) $L_c \ll L_s$ $L_c \ll L_w \to \beta \ll 1$ and $\beta\sqrt{\lambda} \ll 1$;

Regime I

(ii) $L_s \ll L_c$ $L_s \ll L_w \to \beta \gg 1$ and $\lambda \ll 1$;

Regime II

(iii) $L_w \ll L_c$ $L_w \ll L_s \to \beta\sqrt{\lambda} \gg 1$ and $\lambda \gg 1$;

Regime III. (39)

Being aware of the different length scales relevant to each regime, we decided to re-illuminate the original governing equation (4) so as to make an order-of-magnitude analysis between the transient, convection and diffusion terms.

Table 1 summarizes the time and length scales and the renormalized equations corresponding to each regime. In Regime I ($\beta \ll 1$ and $\beta\sqrt{\lambda} \ll 1$), the unsteady term can be dropped out so that the convection term is balanced with the diffusion term. By contrast, the conduction term in Regime II ($\beta \gg 1$ and $\lambda \ll 1$) becomes negligibly small and the unsteady term is comparable to the convection term. It is further noted that β is a predominant parameter. Nevertheless, in Regime III ($\beta\sqrt{\lambda} \gg 1$ and $\lambda \gg 1$), the general behavior is very close to Regime II, but $\beta\sqrt{\lambda}$ is more important than β itself. Due to the presence of λ in the argument of cosine function, $\beta\sqrt{\lambda}$ however is not a unique parameter to control the heat transfer. Table 1 shows that the effect of λ in Regime III is relatively small since $|\cos x| \leqslant 1$. In Regime III it is also notable that $(2L_w)/(\pi\omega L_s)$ was employed as a time scale rather than $1/\omega$. This is because the angular frequency of wall temperature variation experienced by a moving element is not ω but ω (L_s/L_w) due to the periodic distribution of wall temperature. Consequently, the thickness of the thermal boundary layer is determined by $\omega(L_s/L_w)$ and heat transfer is thus controlled by this value.

4. CONCLUSION

It has been investigated how the axially nonlinear wall temperature distribution influences the heat transfer by oscillating pipe flow. In order to do this the temperature

Table 1. Time scales, length scales and renormalized governing equations corresponding to each regime

	Length scale	Time scale	Governing equation	Representative temp. diff.	Wall heat flux	Nusselt number
Regime I	L_c	$\frac{1}{\omega}$	$\beta^2\frac{\partial\theta}{\partial\tau}+\frac{1}{2}\cos\tau\frac{\partial\theta}{\partial x^\circ}=\frac{1}{\eta}\frac{\partial}{\partial\eta}\left(\eta\frac{\partial\theta}{\partial\eta}\right)$	$\frac{1}{24}\beta^4\lambda^2\sin x$	$\frac{1}{8}\beta^4\lambda^2\sin x$	6
Regime II	L_s	$\frac{1}{\omega}$	$\beta^2\frac{\partial\theta}{\partial\tau}+\frac{1}{2}\beta^2\cos\tau\frac{\partial\theta}{\partial x}=\frac{1}{\eta}\frac{\partial}{\partial\eta}\left(\eta\frac{\partial\theta}{\partial\eta}\right)$	$2\lambda^2\sin x$	$\sqrt{2}\beta\lambda^2\sin x$	$\sqrt{2}\beta$
Regime III	L_w	$\frac{2}{\pi}\frac{1}{\omega}\frac{L_w}{L_s}$	$\beta^2\lambda\frac{\partial\theta}{\partial\tau^\circ}+\frac{1}{2}\beta^2\lambda\cos(\tau/\lambda)\frac{\partial\theta}{\partial x^\circ}=\frac{1}{\eta}\frac{\partial}{\partial\eta}\left(\eta\frac{\partial\theta}{\partial\eta}\right)$	$\sin x$	$0.76\beta\sqrt{\lambda}\sin x$	$1.52\beta\sqrt{\lambda}$

field has been obtained especially with a sinusoidal wall temperature distribution. Through the analyses of the section-averaged temperature, the wall heat flux, and the Nusselt number, it has been revealed that the heat transfer is governed by two parameters, namely the dimensionless oscillation frequency and swept length ratio. It is found that the characteristics of heat transfer can be classified into three regimes with respect to these parameters as follows:

Regime I ($\beta \ll 1$ and $\beta\sqrt{\lambda} \ll 1$). Because the effect of unsteady term is small, the quasi-steady assumption is valid.

Regime II ($\beta \gg 1$ and $\lambda \ll 1$). The region affected by conduction effect is confined in the vicinity of wall and the unsteady term is balanced with convection term in the core region. The thickness of thermal boundary layer is determined by oscillation frequency.

Regime III ($\beta\sqrt{\lambda} \gg 1$ and $\lambda \gg 1$). Though the overall characteristics of heat transfer are similar to that of Regime II, the thickness of thermal boundary layer is determined by the product of the oscillation frequency and the swept length ratio rather than by the oscillation frequency itself.

Since the governing equation considered in this study is homogeneous and linear, it allows for the superposition principle to be applicable. Therefore, as long as the model equation used in this study remains valid, the present results are directly applicable to more complicated wall temperature boundaries. This is because a general wall temperature distribution can be expanded in a Fourier series and thus the relevant solutions can be found.

Acknowledgements—This work was supported by Turbo and Power Machinery Research Center at Seoul National University.

REFERENCES

1. P. C. Chatwin, On the longitudinal dispersion of passive contaminant in oscillatory flows in tubes, *J. Fluid Mech.* **71,** 513–527 (1975).
2. E. J. Watson, Diffusion in oscillatory pipe flow, *J. Fluid Mech.* **133,** 233–244 (1983).
3. U. H. Kurzweg and L. Zhao, Heat transfer by high-frequency oscillations: a new hydrodynamic technique for achieving large effective thermal conductivities, *Phys. Fluids* **27,** 2624–2627 (1984).
4. U. H. Kurzweg, Enhanced heat conduction in oscillating viscous flows within parallel-plate channels, *J. Fluid Mech.* **156,** 291–300 (1985).
5. U. H. Kurzweg, Enhanced heat conduction in fluids subjected to sinusoidal oscillations, *Trans. ASME J. Heat Transfer* **107,** 459–462 (1985).
6. D. Gedeon, Mean-parameter modeling of oscillating flow, *Trans. ASME J. Heat Transfer* **108,** 513–518 (1986).
7. K. P. Lee, A simplistic model of cyclic heat transfer phenomena in closed spaces, *Proceedings of the 18th Intersociety Energy Conversion Engineering Conference*, pp. 720–723 (1983).
8. R. A. Peattie and R. Budwig, Heat transfer in laminar, oscillatory flow in cylindrical and conical tubes, *Int. J. Heat Mass Transfer* **32**(5), 923–934 (1989).
9. M. Kaviany, Performance of a heat exchanger based on enhanced heat diffusion in fluids by oscillation: analysis, *Trans. ASME J. Heat Transfer* **112,** 49–55 (1990).
10. A. A. Kornhauser and J. L. Smith, Jr, Heat transfer with oscillating pressure and oscillating flow, *Proceedings of the 24th Intersociety Energy Conversion Engineering Conference*, pp. 2347–2353 (1989).
11. A. C. Wang and J. L. Smith, Jr, The importance of anchoring cylinder wall temperature in Stirling cryocooler, *Proceedings of the 25th Intersociety Energy Conversion Engineering Conference*, pp. 386–391 (1990).
12. G. N. Watson, *A Treatise on the Theory of Bessel Functions* (2nd Edn). Cambridge University Press, Cambridge, U.K. (1944).

APPENDIX

The analysis of heat transfer by oscillatory flow in a pipe having finite wall thickness and constant wall temperature gradient was carried out by Kaviany [9]. The solutions of Kaviany can be rearranged as follows.

The temperature is

$$T-T_0=\begin{cases}\gamma\left(z-z_0+\dfrac{L_s}{2}\,\mathrm{Real}[g_f(\eta)\,e^{i\tau}]\right) & \text{for } 0\leqslant\eta\leqslant 1\\ \gamma\left(z-z_0+\dfrac{L_s}{2}\,\mathrm{Real}[g_w(\eta)\,e^{i\tau}]\right) & \text{for } 1\leqslant\eta\leqslant 1+\delta\end{cases}\tag{A1}$$

in which T_0 is the section-time averaged temperature at $z=z_0$, γ is the axial gradient of the wall temperature distribution and δ is the ratio of the wall thickness to the inner radius of the pipe. The temperature profile functions were obtained as below.

$$g_f=\frac{i\alpha\sqrt{i}I_0(\alpha\sqrt{i})}{(1-Pr)\{\alpha\sqrt{i}I_0(\alpha\sqrt{i})-2I_1(\alpha\sqrt{i})\}}$$

$$\times\left\{1-Pr+Pr\frac{I_0(\alpha\sqrt{\mathrm{i}\eta})}{I_0(\alpha\sqrt{\mathrm{i}})}-A\frac{I_0(\beta\sqrt{\mathrm{i}\eta})}{I_0(\beta\sqrt{\mathrm{i}})}\right\} \quad \text{(A2)}$$

$$g_w=\frac{\mathrm{i}B\alpha\sqrt{\mathrm{i}}I_0(\alpha\sqrt{\mathrm{i}})}{(1-Pr)\{\alpha\sqrt{\mathrm{i}}I_0(\alpha\sqrt{\mathrm{i}})-2I_1(\alpha\sqrt{\mathrm{i}})\}}$$
$$\times\left\{\frac{I_0(\beta\sqrt{\mathrm{i}\sigma}\eta)}{I_1(\beta\sqrt{\mathrm{i}\sigma}(1+\delta))}+\frac{K_0(\beta\sqrt{\mathrm{i}\sigma}\eta)}{K_1(\beta\sqrt{\mathrm{i}\sigma}(1+\delta))}\right\} \quad \text{(A3)}$$

where σ is the thermal diffusivity ratio of fluid to wall and $K_n(z)$ is the second kind of modified Bessel function of order n. The coefficients A and B are given by

$$A=\frac{\mu\sqrt{Pr}\dfrac{I_1(\alpha\sqrt{\mathrm{i}})}{I_0(\alpha\sqrt{\mathrm{i}})}-a\sqrt{\sigma}}{\mu\dfrac{I_1(\beta\sqrt{\mathrm{i}})}{I_0(\beta\sqrt{\mathrm{i}})}-a\sqrt{\sigma}} \quad \text{(A4)}$$

$$B=b-\frac{\mu\dfrac{I_1(\beta\sqrt{\mathrm{i}})}{I_0(\beta\sqrt{\mathrm{i}})}-\mu\sqrt{Pr}\dfrac{I_1(\alpha\sqrt{\mathrm{i}})}{I_0(\alpha\sqrt{\mathrm{i}})}}{\mu\dfrac{I_1(\beta\sqrt{\mathrm{i}})}{I_0(\beta\sqrt{\mathrm{i}})}-a\sqrt{\sigma}} \quad \text{(A5)}$$

$$a=\frac{I_1(\beta\sqrt{\mathrm{i}\sigma})K_1(\beta\sqrt{\mathrm{i}\sigma}(1+\delta))}{I_0(\beta\sqrt{\mathrm{i}\sigma})K_1(\beta\sqrt{\mathrm{i}\sigma}(1+\delta))+I_1(\beta\sqrt{\mathrm{i}\sigma}(1+\delta))K_0(\beta\sqrt{\mathrm{i}\sigma})} \quad \text{(A6)}$$

$$b=\frac{I_1(\beta\sqrt{\mathrm{i}\sigma}(1+\delta))K_1(\beta\sqrt{\mathrm{i}\sigma}(1+\delta))}{I_0(\beta\sqrt{\mathrm{i}\sigma})K_1(\beta\sqrt{\mathrm{i}\sigma}(1+\delta))+I_1(\beta\sqrt{\mathrm{i}\sigma}(1+\delta))K_0(\beta\sqrt{\mathrm{i}\sigma})} \quad \text{(A7)}$$

where μ is the thermal conductivity ratio of fluid to wall. The wall heat flux can be obtained by differentiating equation (A1) with respect to η and evaluating it at $\eta=1$.

To verify the influences of the thermal properties of the wall, we consider the asymptotic behaviors of the section-averaged temperatures and wall heat flux. These behaviors are given in the form of the section averages of g's and the radial gradient of g_f at $\eta=1$.

For small β, $\langle g_f\rangle$, $\langle g_w\rangle$ and g_f' can be approximated as below:

$$\langle g_f\rangle\approx-\tfrac{1}{6}\beta^2+\mathrm{i}\frac{1}{1+Cr} \quad \text{(A8)}$$

$$\langle g_w\rangle\approx\mathrm{i}\frac{1}{1+Cr} \quad \text{(A9)}$$

$$g_f'\approx\frac{1}{2}\frac{Cr}{1+Cr}\beta^2 \quad \text{(A10)}$$

where Cr is defined as

$$Cr\equiv\frac{\sigma\{(\delta+1)^2-1\}}{\mu} \quad \text{(A11)}$$

which is reduced to

$$Cr=\frac{(R_0^2-R^2)\rho_w c_{pw}}{R^2\rho_f c_{pf}} \quad \text{(A12)}$$

and represents the ratio of the thermal capacity of the fluid to the wall at a cross section.

In the limiting case of large β, $\langle g_f\rangle$, $\langle g_w\rangle$ and g_f' can be written as

$$\langle g_f\rangle\approx\mathrm{i} \quad \text{(A13)}$$

$$\langle g_w\rangle\approx\frac{2\sqrt{\mathrm{i}}}{Cr(\sqrt{Pr}+1)}\beta^{-1} \quad \text{(A14)}$$

$$g_f'\approx-\frac{\sqrt{\mathrm{i}^3}}{\sqrt{Pr}+1}\beta \quad \text{for } \sigma/\mu^2\gg 1. \quad \text{(A15)}$$

From the above equations it can be shown that when $Cr\gg 1$ the oscillation of the wall temperature is much smaller than that of the fluid temperature for both limiting cases of small and large β. Since Cr generally has a large number around $10^2\sim10^4$ for a gaseous fluid and a metallic pipe of small radius, the wall temperature can be considered to maintain a constant value with time regardless of the flow oscillation. When β is less than $\sqrt{6/(1+Cr)}$, however, the oscillation of the fluid temperature becomes similar to that of the wall temperature. Hence, the oscillation of the wall temperature cannot be neglected for very slow oscillation in which $\beta<\sqrt{6/(1+Cr)}$.

When β is larger than unity, there can exist a thermal boundary layer within the wall and the inner surface temperature differs from the section-averaged wall temperature if the conductivity of the wall is not sufficiently larger than that of the fluid. The amplitude ratio of the inner surface temperature to the section-averaged fluid temperature can be approximated as

$$\frac{|g_f|_{\eta=1}|}{|\langle g_f\rangle|}\approx\frac{1}{(1+\sqrt{Pr})\sqrt{\sigma/\mu^2}} \quad \text{for } \beta\gg 1. \quad \text{(A16)}$$

However, σ/μ^2 is usually very large for a gaseous fluid and a metallic wall. And thus the variation of the inner surface temperature can be neglected compared with that of the fluid.

The above equations can be also utilized to shed light on the influence of the Prandtl number. As shown in equations (A8)–(A10), Pr has a completely diminishing influence for small β. But when β is more or less above the unity, the characteristics of heat transfer are affected by the value of the Prandtl number. The influence of the Prandtl number, however, is meager for $Pr<1$, because of the dependence on $1/(1+\sqrt{Pr})$, as can be seen in equations (A14) and (A15). Therefore the case of $Pr\lesssim 1$ might be approximated as the case of a vanishing Pr.